Hygrothermal Investigation of Facade Panel Connections Using a Transient Coupled Heat and Moisture Transport Model

B. Abediniangerabia[1] and S.M. Shahandashti[2]
1. Department of Civil Engineering, The University of Texas at Arlington, Arlington, TX, United States; Email: bahram.abediniangerabi@uta.edu
2. Department of Civil Engineering, The University of Texas at Arlington, Arlington, TX, United States; Email: mohsen@uta.edu– corresponding author

Abstract: In this paper, a coupled three-dimensional heat and moisture transfer model in the transient state was used to investigate the effect of panel connections on the hygrothermal performance of innovative façade panels. For this purpose, two panel corner connections proposed by Precast/Prestressed Concrete Institute (PCI) were selected and modeled in COMSOL Multiphysics to illustrate the moisture and heat behaviors within the corner connections of the innovative UHP-FRC facade panels. The results of heat transfer analysis showed that steel connections could significantly reduce the thermal resistivity of façade panels by converging heat fluxes and acting as thermal bridges within façade panels. Also, the results of moisture transfer showed that air gaps at the corner had higher moisture flux compared to the other layers in the models. The results show the significant importance of connections in the energy performance analysis of façade systems. They also highlight the importance of devising novel connection designs and materials that consider the transient, coupled heat and moisture transfer in the connections to effectively exploit the potential opportunities provided by innovative materials to improve building energy efficiency.

Keywords: Facade panel connections, Coupled heat and moisture transfer, Transient state, UHP-FRC facade panel, Hygrothermal performance

1. Introduction

Building facade systems are the main component of a building that receives external heat and moisture gains or loses internal heats [1]. Therefore, it is essential to improve their energy efficiency to reduce building energy consumptions. In recent years, several innovative solutions have been proposed to develop energy-efficient façade systems, such as double-skin facades [2], [3], phase-change materials [4], building integrated photovoltaic (BIPV) [5], and ultra-high-performance fiber-reinforced-concrete (UHP-FRC) facade panel [6], [7], [8], [9], and [10]. There are also several studies conducting investment evaluation of innovative solutions for façade systems signifying their significance impacts in the building sector [11], [12], and [13]. Although these innovative materials and facades offer higher energy efficiencies, the effect of panel connections in the energy performance analysis of these innovative facade systems have been overlooked. Thermal bridges in the facade systems can accelerate heat transfer between indoor and outdoor environments resulting in heat loss in the buildings. Wall framings and connections are examples of such components in a facade system that may penetrate insulation layers and create point and linear thermal bridging. Similarly, vapor condensation may occur within building facade systems and their connections due to different ambient conditions between the indoor and outdoor environments [14], which can decrease the service life of the system by degrading materials and increase the risk of mold growth within facade systems. Therefore, it is essential to investigate the heat and moisture transfer within the facade connections.

Some rare studies investigated the hygrothermal performance of building facade systems by coupling heat and moisture transfer. For example, Ibrahim et al. [15] used one-dimensional coupled heat and moisture transfer analysis to investigate the hygrothermal performance of different wall structures with an insulating layer. Similarly, Xua & Lia [16] investigated the condensation characteristics of thermal insulation walls in hot and humid areas in China using a 1-D coupled heat and moisture transfer model. More recently, Fang et al. explored the impact of climate change on cooling loads transmitted within multi-layer walls in the hot and humid southern China [17]. These studies are mostly based on one-dimensional hygrothermal models, which are limited in investigating real-world applications, such as heat and moisture transfer within complex wall framing and facade panel connections.

In this paper, the effect of panel connections on the hygrothermal performance of façade panels was investigated using a coupled three-dimensional heat and moisture transport in the transient state.

2. Methodology

Heat and moisture transfer processes in porous construction materials were modeled as a system of two partial differential equations, which derived by imposing the equilibrium balance of mass and energy within a representative elementary volume. Two panel corner connections proposed by Precast/Prestressed Concrete Institute (PCI) [18] were selected as examples to illustrate the effect of panel connections on the hygrothermal performance of innovative UHP-FRC facade panels. Figure 1 shows the cross-section and 3D views of these panel corner connections.

COMSOL Multiphysics was used to model and solve the numerical models. COMSOL Multiphysics is a well-suited solver for simulating 3D models as well as solving Multiphysics problems for building physics [19]. COMSOL Multiphysics provides a powerful interactive environment for Multiphysics modeling and solving scientific and engineering problems [20]. COMSOL Multiphysics enables users to easily set design parameters, create meshes, and visualize the simulation results for post-processing operations.

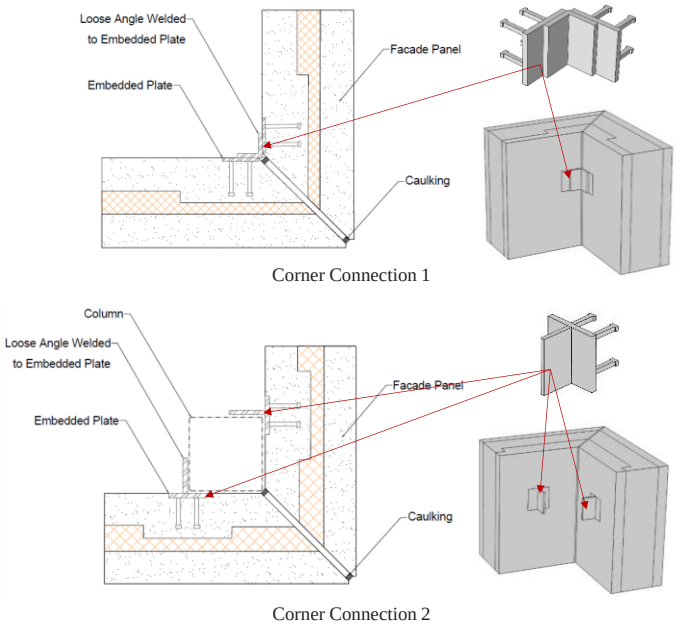

Figure 1. Cross-section and 3D views of the UHP-FRC corner connections

2.1. Governing Equations

Governing equations of coupled moisture and energy transfer in building porous materials can be formulated based on the principle of the preservation of the combined heat and humidity of a representative elementary volume [21]. Moisture can transfer within building materials in both phases of liquid and vapor [22]. Vapor transfers by diffusion due to the pressure gradient and also by convection due to airflow within the porous media. Moisture in the form of liquid also flows due to moisture content gradient, and moisture conduction occurs due to moisture diffusivity as the driving potential [21].
In this paper, the air transfer is formulated implicitly in the mass and heat conservation equations, and it is assumed that the airflow is constant and moisture content independent. Therefore, the governing equations of moisture and heat transfer in a one-dimensional form can be formulated by the following partial differential equations, respectively [10]:

$$\frac{\partial w}{\partial \varphi}\frac{\partial \varphi}{\partial t} = \nabla \cdot (K_l \nabla P_C) + \nabla \cdot \delta_P \left(\frac{P_v}{P_l}\nabla P_C + \left(\varphi \frac{\partial P_{sat}}{\partial T} - \frac{P_v ln\varphi}{T}\right)\nabla T\right) - v \cdot \nabla \rho_v \quad (1)$$

where v is the airflow velocity (m/s), w is moisture content (kg/m^3), φ is relative humidity (-), K_l is liquid water permeability (m^2), P_C is the capillary pressure (Pa), P_l is liquid water pressure (Pa), P_v is the partial water vapor pressure (Pa), δ_P is the vapor permeability (kg/m s Pa), ρ_v is the water vapor density (kg/m^3), and t is the time (s).

$$(\rho C_p)_{eff}\left(\frac{\partial T}{\partial t}\right) = \nabla \cdot (k_{eff} . \nabla T) + L_v \nabla \cdot (\delta_P \nabla p_V) - v \cdot (L_v \nabla p_V + \rho_a C_{P,a} \nabla T) \quad (2)$$

where L_v is the latent heat from vaporization (J/kg), ρ_a is dry air density (kg/m^3), and $C_{P,a}$ is the heat capacity of dry air (J/kgK). The effective volumetric capacity at constant pressure and effective thermal conductivity are described as follows, respectively:

$$(\rho C_p)_{eff} = \rho_s C_{p,s} + w C_{p,w} \quad (3)$$

$$k_{eff} = k_s\left(1 + \frac{bw}{\rho_s}\right) \quad (4)$$

where ρ_s is the dry solid density (kg/m^3), $C_{p,s}$ is the dry solid specific heat capacity (J/kgK), w is the water content (kg/m^3) from moisture storage function for the selected material, $C_{p,w}$ is the water heat capacity in constant pressure (J/kgK), k_s is the dry solid thermal conductivity (W/mK), and b is the thermal conductivity supplement due to water content.
Equations (1) and (2) were implemented in COMSOL Multiphysics in the form of a coupled heat and moisture transfer (HAM) for porous materials in a transient state (i.e., time-dependent).

2.2. Boundary Conditions, Initial Conditions, and Material Thermophysical Properties

Boundary conditions for heat transfer at both sides of a multilayer facade panel were described by the following equation in terms of convection heat flux:

$$q = a(T_{air} - T_{surface}) \quad (3)$$

where q is the heat flux density (W/m^2) in the external and internal panel surfaces, a is the total heat transfer coefficient (W/m^{2}K), T_{air} is the ambient air temperature (K), and $T_{surface}$ is the surface temperature of the panel material (K). Similarly, boundary conditions for moisture transfer at both sides of the multilayer facade panel were described by the following equation in terms of convection moisture flux and pressure difference.

$$g = \beta(p_{air} - p_{surface}) \quad (4)$$

where g is the vapor diffusion density (kg/m^{2}s) in the external and internal panel surfaces, β is the water vapor transfer coefficient (kg/m^{2}sPa), p_{air} is the partial pressure of water vapor in the ambient air (Pa), and $p_{surface}$ is the partial pressure of the building material (Pa).
Table 1 presents the interior and exterior boundary conditions considered for this study. The interior surface of the models was exposed to the indoor fixed temperature of 292.15 K (19 °C) with the convective heat transfer coefficient of 5 W/m^{2}K and moisture transfer coefficient of 8e-8 s/m. The exterior surface of the models was exposed to ambient temperature and ambient relative humidity with the convective heat transfer coefficient of 25 W/m^{2}K and moisture transfer coefficient of 25e-8 s/m. The influence of radiation and rain were excluded from the study for simplicity. The meteorological data for Miami International Airport (ASHRAE) [23] was used in the simulation to provide ambient temperature and relative humidity. The simulations were carried out for three months between June and August 2017.

Table 1: Boundary conditions

Parameter	Unit	Interior	Exterior
θ	K (°C)	292.15 K (19 °C)	T(t)
φ	%	50	φ(t)
α	W/m^{2}K	5	25
β	s/m	8e-8	25e-8

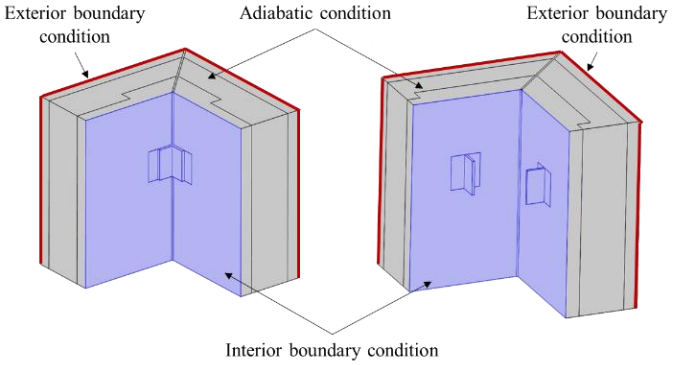

Figure 2. Graphical representation of boundary conditions for panel corner connections

Initial temperature and relative humidity inside construction materials were assumed 292.15 K (19 °C) and 50%, respectively. Table 2 shows the thermal and hygrothermal properties of the UHP-FRC panel and connections used in the numerical simulations. Figure 3 illustrates the moisture functions of UHP-FRC and XPS.

Table 2: Thermo-physical properties of UHP-FRC panel assembly and steel connection

Materials	Parameters	Unit	Values*
Concrete layer (UHP-FRC)	Thickness (D)	cm	3.81 (1.5 in)
	Density (ρ)	kg/m^3	2403
	Porosity (P)	m^3/m^3	0.7912
	Specific heat capacity (Cp)	J/kgK	1010
	Thermal conductivity (λ)	W/mK	$\lambda(\varphi)$
	Vapor diffusion resistance (μ)	-	18.58
	Moisture content (MC)	kg/m^3	$w(\varphi)$
Insulation layer	Thickness (D)	cm	12.7 (5 in)
	Density (ρ)	kg/m^3	20
	Porosity (P)	m^3/m^3	0.99
	Specific heat capacity (Cp)	J/kg K	645
	Thermal conductivity (λ)	W/m K	0.005769
	Vapor diffusion resistance (μ)	-	170.55
	Moisture content (MC)	kg/m^3	$w(\varphi)$
Panel Layers Connectors (Fiberglass)	Density (ρ)	kg/m^3	91.4
	Specific heat capacity (Cp)	J/kg K	$c_p(T)$
	Thermal conductivity (λ)	W/m K	$\lambda(T)$
Connection (Steel)	Density (ρ)	kg/m^3	$\rho(T)$
	Specific heat capacity (Cp)	J/kg K	$c_p(T)$
	Thermal conductivity (λ)	W/m K	50.2

Note: f(x) indicates that the parameter x is dependent on another parameter.

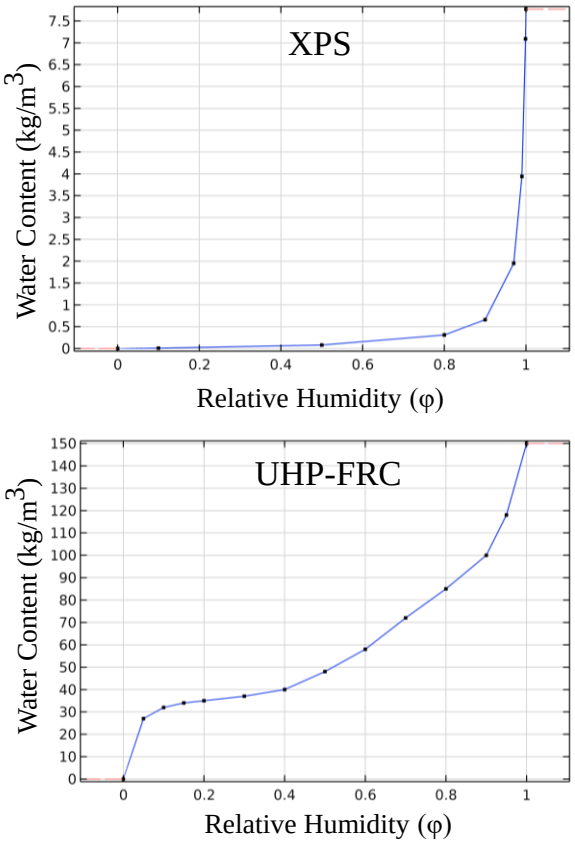

Figure 3. Moisture functions of UHP-FRC and XPS

2.3. Sensitivity Analysis

The sensitivity of the proposed coupled heat and moisture model was investigated regarding variation in moisture and heat transfer coefficients of exterior boundary conditions. Table 3 shows the variation of both moisture and heat transfer coefficients from reference values. Case A represents the model with 70% of the reference heat and moisture transfer coefficients. Case B represents the reference model with the reference heat and moisture transfer coefficients. And, Case C represents the model with 130% of the reference heat and moisture transfer coefficients.

Table 3: Variation of heat and moisture transfer coefficients from reference values

Parameter	-30% (Case A)	Reference (Case B)	+30% (Case C)
α (W/m^{2}K)	17.5	25	32.5
β (s/m)	175e-9	25e-8	325e-9

2.4. Solver Setting and Spatial Discretization

A time-dependent solver was selected for both studies with a relative tolerance of 0.01. Non-structured and non-uniform tetrahedral meshes were generated using the COMSOL auto mesh generator for both studies. Figure 4 shows the meshes generated for the panel connections. The meshes for Type 1 and Type 2 connections were composed of 26124 and 26873 tetrahedral elements, respectively. Type 1 and Type 2 models presented 73400 and 69460 degrees of freedom, respectively. The simulation of each study for three months (Summer 2017) took about 9 hours to obtain the solutions for the system with the following configurations: Intel(R) Core i7-3770 CPU, 3.40 GHz, Quad-Core, and 16GB RAM.

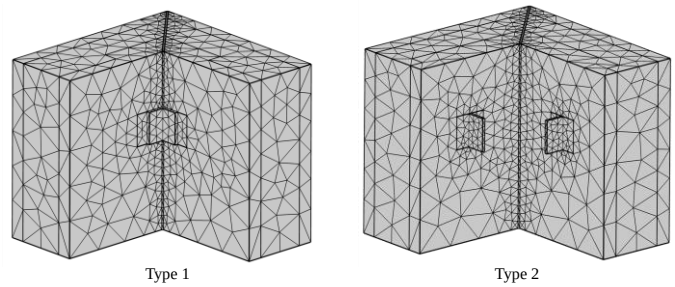

Figure 4. Meshes generated for panel connections

3. Simulation Results

3.1. Results of Heat Transfer

Figure 5 illustrates the temperature distribution within the cross-section of both panel corner connections at the location of steel connectors. This figure shows that the insulation layers in both connection types could regulate the temperature distribution within the cross-sections. Although steel connectors have lower thermal resistivity compared to concrete and insulation layers, they do not often interfere with the temperature distribution within these connections since they have placed on the interior side of the insulation layer only. However, it is shown that the temperature in the interior side of the Type 1 connection is higher (about two Kelvin) in comparison with the temperature in the interior side of the Type 2 connection.

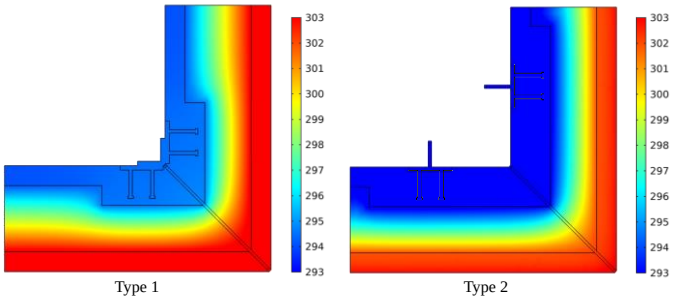

Figure 5. Temperature distribution within the cross-section of both panel corner connections on July 31st

Figure 6 illustrates heat fluxes magnitude within the cross-section of both corner connections at the location of steel connectors on July 31st. This figure shows how the steel connector at the corner of Type 1 connection reduces the thermal resistivity within facade panels by converging heat fluxes and acting as a thermal bridge. In comparison, the steel connectors in the Type 2 connection seem to not have a huge impact on heat fluxes within the facade panel. Comparing the heat flux magnitude within both cases shows that the steel connector of Type 1 connection has a higher magnitude (about 360 W/m^2 intensity). On the other hand, steel connectors in the Type 2 connection have much lower magnitudes (about 15 W/m^2 intensity). Figure 7 clearly illustrates how steel connectors can redirect heat flux vectors within panel connections due to their low thermal resistivity.

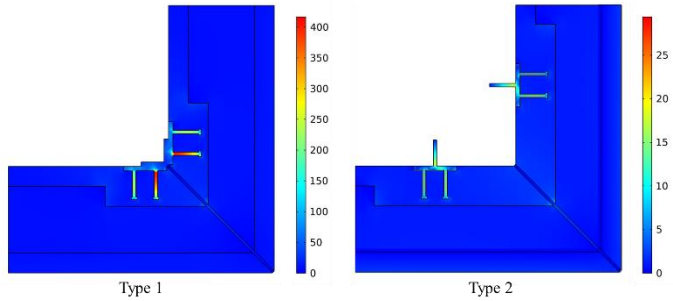

Figure 6. Heat flux magnitude within the cross-section of both panel corner connections on July 31st

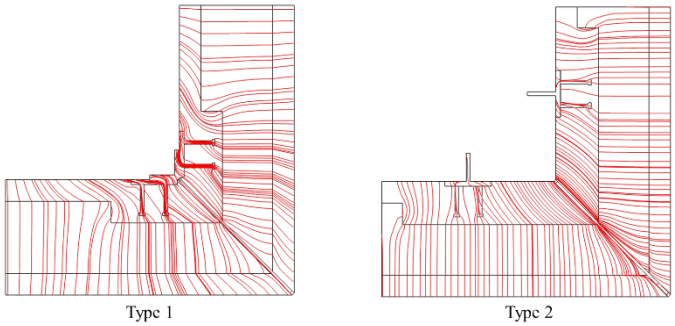

Figure 7. Streamlines of heat flux within the cross-section of both panel corner connections on July 31st

3.2. Results of Moisture Transfer

Figure 8 illustrates the relative humidity within the cross-section of both panel corner connections at the location of steel connectors on July 31st. Comparing relative humidity within both panel corner connections clearly shows higher relative humidity in Type 1 connection than the relative humidity in Type 2 connection. The relative humidity within the Type 2 connection seems consistent across the cross-section. However, very high relative humidity (more than 80%) is shown behind the steel connector at the corner of the Type 1 connection. The moisture flux vectors shown in Figure 9 indicate that the air gap at the corner of both panel connections is responsible for the moisture transfer from the exterior side toward the interior side. However, the moisture gets trapped behind the steel connector in the Type 1 connection resulting in moister content increase. In contrast, there is no such increase in moisture content in the Type 1 connection.

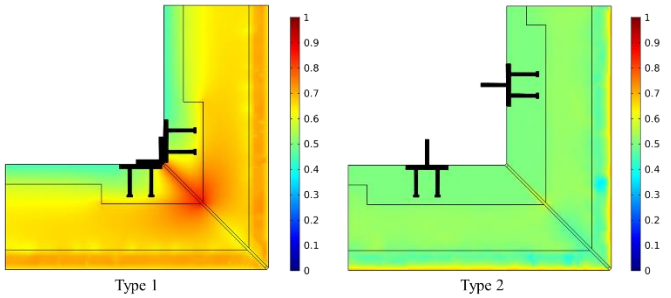

Figure 8. Relative humidity within the cross-section of both panel corner connections on July 31st

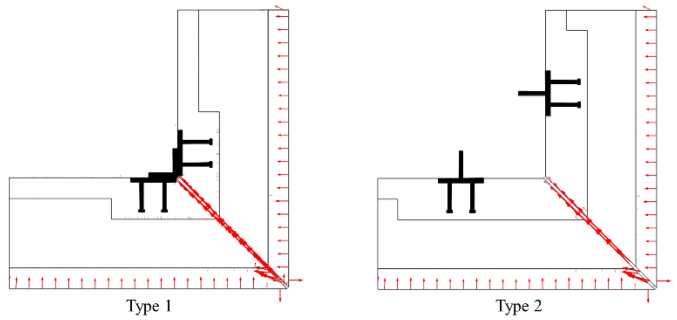

Figure 9. Moisture flux vectors within the cross-section of panel connections on July 31st

The results of moisture transfer within the cross-section of Type 1 connection showed a high percentage of relative humidity (above 80%) behind the steel connector at the corner highlighting the criticality of this location. Excessive moisture can increase the risk of mold growth within the building materials [19]. Therefore, the relative humidity and temperature fluctuations were monitored for a longer period (three months – from June 2017 to August 2017) at the corner of both connections (Figure 10) to evaluate the risk of mold growth for both panel connections.

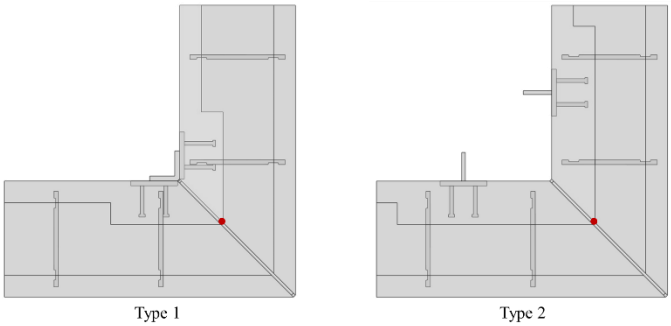

Figure 10. Location of point probes at the cross-section of panel connections

A long-run exposer to a high level of relative humidity (i.e., 80%) is considered as the lowest possible relative humidity required for mold growth for very sensitive building materials, such as wood and timber [24]. This level could be slightly higher (e.g., 85%) for less sensitive materials, such as concrete and insulation material [24].

Figure 11 illustrates the temperature and relative humidity at the corner of Type 1 connection. This figure clearly shows that the relative humidity passes the threshold (i.e., 85%) at 294.9 K (21.75 °C) and reaches to 92.5%. This high range of relative humidity at the temperature of around 294.15 K (21°C) indicates a high risk of mold growth at the corner of the connection.

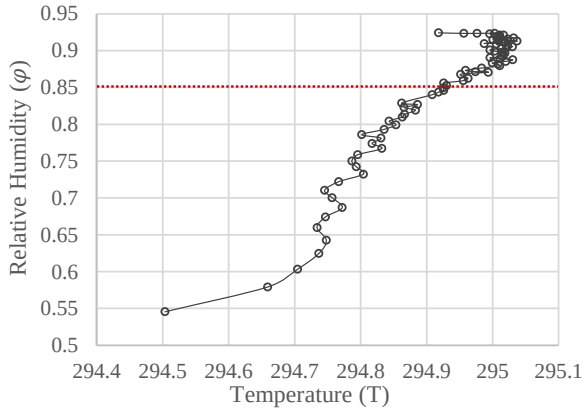

Figure 11. Temperature and relative humidity at the corner of the Type 1 connection during Summer 2017 (3 months)

Figure 12 illustrates the temperature and relative humidity at the corner of Type 2 connection. This figure shows that the relative humidity can only reach up to 61%, which is not critical for mold growth. Therefore, the risk of mold growth at the corner of Type 2 connection is almost zero.

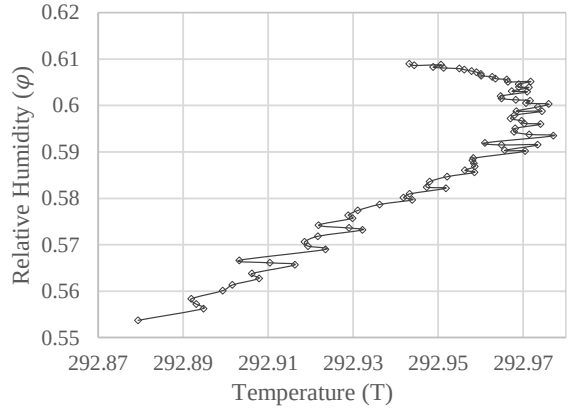

Figure 12. Temperature and relative humidity at the corner of the Type 2 connection during Summer 2017 (3 months)

3.3. Results of Sensitivity Analysis

The sensitivity of the model was investigated concerning two input parameters (i.e., heat and moisture transfer coefficients) for both panel connections. Figure 13 illustrates the relative humidity and temperature at the corner of the Type 1 connection for 90 days (June 2017 to August 2017). The results show that the variation of both parameters slightly affects the relative humidity and temperature at the corner.

Considering the fluctuation in the relative humidity and temperature at the corner of the Type 2 connection (Figure 14) also indicates that a 30% variation in heat and moisture transfer coefficients on the exterior boundary condition has a slight impact on the relative humidity and temperature at the corner.

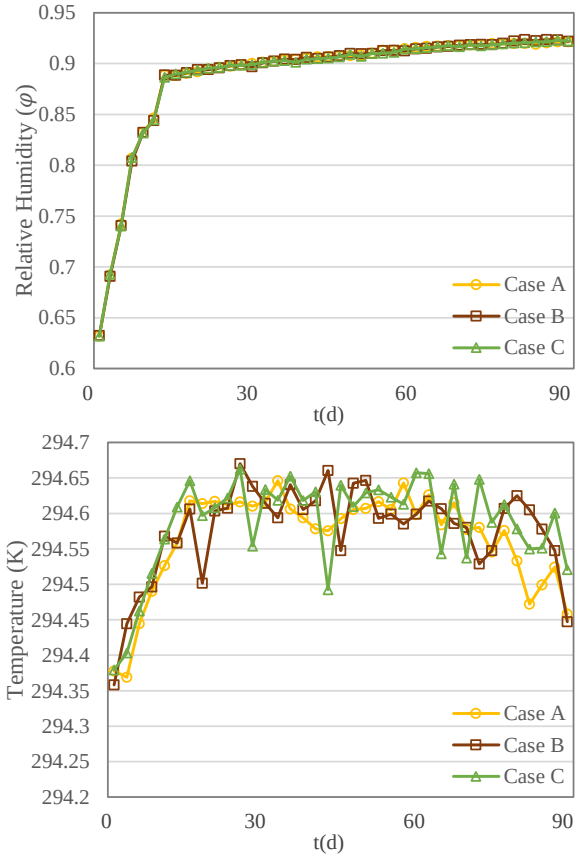

Figure 13. Relative humidity and temperature at the corner of Type 1 connection during Summer 2017 (90 days)

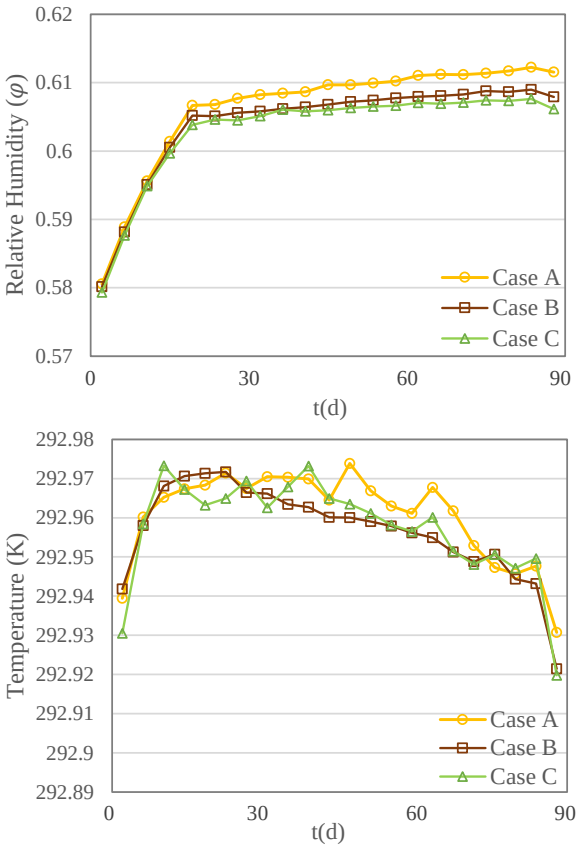

Figure 14. Relative humidity and temperature at the corner of Type 2 connection during Summer 2017 (90 Days)

4. Conclusions

In this paper, a coupled transient heat and moisture transfer model was developed to evaluate the heat and moisture behavior within two different panel corner connections proposed by the Precast/Prestressed Concrete Institute (PCI). COMSOL Multiphysics was used to solve the numerical models. The results showed that using a single steel connector (e.g., Type 1 connection) can drastically reduce the thermal resistivity of panels since it acts as a thermal bridge accelerating heat loss through panels. It is also shown that moisture gets trapped behind the steel connector in Type 1 connection results in high relative humidity at the corner, which increases the risk of mold growth by providing ideal conditions for germination. On the other hand, Type 2 connection offers higher performance regarding thermal bridging and the risk of mold growth.

The sensitivity of the coupled transient heat and moisture transfer model was investigated concerning heat and moisture transfer coefficients of exterior boundary conditions for both panel connections. The results of the sensitivity analysis indicated that the variation of both input parameters has a slight impact on the relative humidity and temperature at the corner of both connections.

The results presented in this study showed the significant importance of panel connections in the energy performance analysis of facade systems. However, further studies are needed to focus on investigating the hygrothermal performance of other types of panel connections, such as shear wall panels and load-bearing panel connections. Moreover, the simulations in this study were carried out only for limited duration and weather conditions. Future studies are required to investigate the hygrothermal performance of panel connections in different weather conditions and for the whole year.

5. References

[1]. Jiru, T. E., Tao, Y. X., & Haghighat, F., Airflow and heat transfer in double skin facades, *Energy and Buildings*, **43(10)**, 2760-2766 (2011)

[2]. Agathokleous & Kalogirou, S. A., Double skin facades (DSF) and building-integrated photovoltaics (BIPV): A review of configurations and heat transfer characteristics, *Renewable Energy*, **89**, 743-756 (2016)

[3]. Ghaffarianhoseini, A., Ghaffarianhoseini, A., Berardi, U., Tookey, J., Li, D. H. W., & Kariminia, S., Exploring the advantages and challenges of double-skin facades (DSFs). *Renewable and Sustainable Energy Reviews*, **60**, 1052-1065 (2016)

[4]. De Gracia, A., & Cabeza, L. F., Phase change materials and thermal energy storage for buildings. *Energy and Buildings*, **103**, 414-419 (2015)

[5]. Cucchiella, F., D'Adamo, I., & Koh, S. L., Environmental and economic analysis of building integrated photovoltaic systems in Italian regions. *Journal of Cleaner Production*, **98**, 241-252 (2015)

[6]. Abediniangerabi, B., Shahandashti, S. M., & Makhmalbaf, A., Coupled transient heat and moisture transfer investigation of facade panel connections, *Journal of Engineering, Design and Technology*, Emerald Publishing (2019)

[7]. Abediniangerabi, B., Shahandashti, S. M., Bell, B., Chao, S. H., & Makhmalbaf, A., Assembly-Scale and Whole-Building Energy Performance Analysis of Ultra-High-Performance Fiber-Reinforced Concrete (UHP-FRC) Facade Systems, In *International Interactive Symposium on Ultra-High Performance Concrete*, **Vol. 2, No. 1**. Iowa State University Digital Press (2019)

[8]. Abediniangerabi, B., Shahandashti, S. M., Bell, B., Chao, S. H., & Makhmalbaf, A., Building energy performance analysis of ultra-high-performance fiber-reinforced concrete (UHP-FRC) facade systems, *Energy and Buildings*, **174**, 262-275 (2018)

[9]. Shahandashti, S. M., Abediniangerabi, B., Bell, B., & Chao, S. H., Probabilistic Building Energy Performance Analysis of Ultra-High-Performance Fiber-Reinforced Concrete (UHP-FRC) Façade System, In *Computing in Civil Engineering 2017*, pp. 223-230 (2017)

[10]. Abediniangerabi, B., Assembly-Scale and Whole-Building Energy Performance Analysis of Ultra-High-Performance Fiber-Reinforced Concrete (UHP-FRC) Facade Systems, Doctoral Dissertation, University of Texas at Arlington (2019)

[11]. Shahandashti, M., Ashuri, B., and Mostaan, K., Automatic fault detection for Building Integrated Photovoltaic (BIPV) systems using time series methods. *Built Environment Project and Asset Management* (2018)

[12]. Kashani, H., Ashuri, B., Lu, J., & Shahandashti, M., A real options model to evaluate investments in photovoltaic (PV) systems. In *Construction Research Congress 2012*: Construction Challenges in a Flat World (pp. 1641-1650). (2012)

[13]. Shahandashti, S. M., Mostaan, K., & Ashuri, B., Methods for Assessing Longitudinal Variations of Energy Production by PV Systems. In *AEI 2013: Building Solutions for Architectural Engineering* (pp. 113-122). (2013)

[14]. Qin, M., Belarbi, R., Aït-Mokhtar, A., & Nilsson, L. O., Coupled heat and moisture transfer in multi-layer building materials, *Construction and Building Materials*, 23(2), 967-975 (2009)

[15]. Ibrahim, M., Wurtz, E., Biwole, P. H., Achard, P., & Sallee, H., Hygrothermal performance of exterior walls covered with aerogel-based insulating rendering, *Energy and Buildings*, **84**, 241-251 (2014)

[16]. Xua, C., & Lia, S., Simulation research on the condensation characteristics of thermal insulation walls with a vapour barrier, *Energy Procedia* (2019)

[17]. Fang, A., Chen, Y., & Wu, L., Transient simulation of coupled heat and moisture transfer through multi-layer walls exposed to future climate in the hot and humid southern China area, *Sustainable Cities and Society*, **52**, 101812 (2020)

[18]. Losch, E. D., Hynes, P. W., Andrews Jr, R., Browning, R., Cardone, P., Devalapura, R., & Kourajian, P., State of the art of precast/prestressed concrete sandwich wall panels, *PCI Journal*, **56(2)**, 131-176 (2011)

[19]. Baghban, M. H., Hovde, P. J., & Gustavsen, A., Numerical simulation of a building envelope with high performance materials, In *COMSOL Conference.* Paris (2010)

[20]. Huang, Z., Conway, P. P., Thomson, R. C., Dinsdale, A. T., & Robinson, J. A., A computational interface for thermodynamic calculations software MTDATA. *Calphad*, **32(1)**, 129-134 (2008)

[21]. Maliki, M., Laredj, N., Bendani, K., & Missoum, H., Two-dimensional transient modeling of energy and mass transfer in porous building components using COMSOL Multiphysics, *J. Appl. Fluid Mech*, **10**, 319-328 (2017)

[22]. Balocco, C. and Petrone, G., Mathematical Modelling of Engineering Problems, Journal homepage: http://iieta. org/Journals/MMEP, **5(3)**, 146-152 (2018)

[23]. Roth, M., Updating the ASHRAE Climate Design Data for 2017, *ASHRAE Transactions*, **123** (2017)

[24]. Ojanen, T., Viitanen, H., Peuhkuri, R., Lähdesmäki, K., Vinha, J., & Salminen, K., Mold growth modeling of building structures using sensitivity classes of materials, *Proceedings Buildings XI, Florida* (2010)